Seismic Fragility Analysis of a Coupled Tank-Piping System based on Artificial Ground Motions and Surrogate Modeling

G. Abbiati*[1], M. Broccardo[2], R. di Filippo[2], B. Stojadinovic[3], and O.S. Bursi[2]

[1]*Department of Engineering, Aarhus University, Denmark*
[2]*Department of Civil, Environmental and Mechanical Engineering, University of Trento, Italy*
[3]*Department of Civil, Environmental and Geomatic Engineering, ETH Zurich, Switzerland*

Draft submitted to *engrXiv*

November 20, 2020

Abstract

The catastrophic consequences of recent *NaTech* events triggered by earthquakes highlighted the inadequacy of standard approaches to seismic risk assessment of chemical process plants. To date, the risk assessment of such facilities mainly relies on historical data and focuses on uncoupled process components. As a consequence, the dynamic interaction between process equipment is neglected. In response to this gap, researchers started a progressive integration of the Pacific Earthquake Engineering Research Center (PEER) Performance-Based Earthquake Engineering (PBEE) risk assessment framework. However, a few limitations still prevent a systematic implementation of this framework to chemical process plants. The most significant are: i) the computational cost of system-level simulations accounting for coupling between process equipment; ii) the experimental cost for component-level model validation; iii) a reduced number of hazard-consistent site-specific ground motion records for time history analyses.

In response to these challenges, this paper proposes a recently developed uncertainty quantification-based framework to perform seismic fragility assessments of chemical process plants. The framework employs three key elements: i) a stochastic ground-motion model to supplement scarcity of real records; ii) surrogate modeling to reduce the computational cost of system-level simulations; iii) a component-level model validation based on cost-effective hybrid simulation tests. In order to demonstrate the potential of the framework, two fragility functions are computed for a pipe elbow of a coupled tank-piping system.

Keywords: Seismic fragility analysis; PEER-PBEE framework; Artificial ground motion; Surrogate modeling; Hybrid simulation; Tank-piping system.

1 Introduction

Campedel [1] showed that natural hazards are one the leading cause of Chemical Process Plants (CPP) accidents. The study is based on an extensive review of historical data based on five European and one US databases. Kidam and Hurme [2] found similar figures by analyzing 364 CPP accidents from the Japanese Failure Knowledge Database. Such occurrences are classified as *NaTech* events, that is, technological accidents triggered by natural disasters. Release of hazardous chemicals, fire, or explosions following a structural failure are often among the most significant consequences of NaTech events [3, 4]. The Izmit refinery fire following the Kocaeli earthquake (Turkey, 1999) [5], the leak of hazardous chemicals from multiple fertilizer plants following the Wenchuan earthquake (China, 2008) [6], and the nuclear accident following the Fukushima earthquake-induced Tsunami (Japan, 2011) [7] are just some examples of NaTech events associated with seismic hazard.

Their catastrophic consequences have highlighted the inadequacy of standard approaches to risk assessment of CPPs. These approaches mainly relies on expert opinion or historical data [8, 9, 10, 11]. Moreover, they are performed at the component level; thus, neglecting system-level interactions with other CPP components [12]. This lack of system-level numerical simulations has been recognized as one of the major research gaps in the current literature.

*Corresponding Author: Dr. Giuseppe Abbiati, abbiati@eng.au.dk, ORCID: 0000-0002-5048-8505.

In response to this research gap, in the last decade, researchers started a progressive integration of performance-based risk analysis frameworks [13]. In the seismic risk context, the natural choice was directed towards the PEER-PBEE approach [14, 15]. In essence, the PEER-PBEE framework uses the total probability theorem to decompose the quantification of seismic risk into different tasks, which can be handled by different groups of experts. In detail, the tasks are: i) probabilistic seismic hazard analysis (PSHA); ii) fragility analysis; iii) damage analysis[†]; iv) loss analysis.

Within this perimeter, fragility analysis of CPPs has become an active research field. As an example, Hosseini *et.al.* [16] computed fragility surfaces for oil refinery piping systems, and Mebarki *et.al.* [17] derived fragility and recovery functions for atmospheric industrial tanks. In addition, different research groups developed system-level numerical simulations for fragility analysis of liquefied natural gas plants [18, 19, 20]. Finally, examples of coupled analysis can be found in [21, 22, 23]. In all these cases, fragility functions are evaluated using a set of suitable ground motions, which are used as input for nonlinear structural analysis [24, 25, 26].

In the context of seismic fragility, Bradley [27] and *et al.* [28] collected a number of open issues. Although both studies refer to the seismic risk of civil structures, their conclusions are also valid for CPPs. Specifically, the authors highlighted the following three criticalities:

- Although methodologies for ground motion selection succeed in describing seismic hazard for a given structural system, the number of available records is usually too small for computing accurate statistics of response quantities of interest (QoI).
- Experimental validation of system components is often overlooked, and this is due to practical reasons. Structural testing is usually not affordable beyond the component level due to the limited capacity of experimental facilities.
- The computation of fragility analysis requires a large number of time history analyses. It follows that computational expensive structural simulators limit *de facto* the total number of simulations.

Recently, Abbiati *et al.* [29] proposed a comprehensive framework that tackles these open challenges. This study adopts and applies this framework to compute the seismic fragility analysis of a tank-piping system of an ideal CPP.

The building blocks of the computational framework are an artificial ground motion (AGM) model calibrated against hazard-compatible site-specific seismic records (e.g., the AGM model of Rezaian and Der Kiureghian in this study [30]), a high-fidelity (HF) structural simulator of the reference structure *validated* against experiments (e.g., hybrid simulation, HS, in the proposed application [31]), and a corresponding low-fidelity (LF) structural simulator (e.g., obtained via dynamic substructuring of the HF structural simulator [32]). The seismic fragility analysis follows these sequential steps: i) generation of an ensemble of AGMs compatible with the seismic hazard, ii) computation of a Polynomial Chaos Expansion (PCE) surrogate of the QoI prediction provided by the LF structural simulator, iii) calculation of PCE-based Sobol' sensitivity indices of the LF-based QoI w.r.t. the ground motion parameters, iv) dimensionality reduction of the parameter space of the AGM model, v) computation of a hierarchical kriging (HK) surrogate that fuses LF and HF realizations of the QoI, vi) fragility analysis computed via Monte-Carlo-based UQ forward analysis of the HK surrogate.
Fragility analysis and, more broadly, seismic risk assessment based on stochastic simulations and Kriging surrogate modeling was firstly proposed in [33] and, more recently, adopted in [34]. Unlike [33, 34], Abbiati *et al.* [29] introduced global sensitivity analysis based on PCE and HK to reduce further the computational cost of the fragility analysis. The resulting framework integrates state-of-the-art know-how in ground motion selections and follows the original spirit of the PEER-PBEE framework, which decouples hazard and fragility analysis.

This paper is organized as follows. Section 2 introduces the proposed seismic fragility analysis framework. Section 3 describes the tank-piping system case study, along with both HF and LF structural simulators. Section 4 describes the AGM model and the related calibration based on real records. Section 5 presents the validation of the HF based on a HS experimental campaign performed at the University of Trento, Italy. Section 6 discusses the results of the seismic fragility analysis of the tank-piping system. Finally, Section 7 summarizes the conclusions of this study.

2 Computational framework for fragility analysis

The theoretical framework is based on the work described in [29]. In order to present a self-contained study, the main parts of the methodology are described below. For further details, the reader should consult the stated

[†]Oftentimes damage analysis and fragility analysis are blended in one assessment

reference. Following [29], a seismic ground motion is represented by a parametric stochastic process, $A(t)$. Two sources of uncertainties are here considered. An epistemic (reducible) uncertainty related to the parameters of the process and an aleatory (irreducible) uncertainty related to the inherent variability of the motion. This process can be written as follow

$$A(t) = \mathcal{M}_a(t, \boldsymbol{Z}|\boldsymbol{X}_a), \tag{1}$$

where $\mathcal{M}_a(\cdot)$ is the synthesis model, $\boldsymbol{Z}$ is a set of random variables representing the aleatory variability, and $\boldsymbol{X}_a$ a is a set of random model parameters.

Let $Y = \mathcal{M}_c(A(t)|\boldsymbol{x}_c)$ being the Quantity of Interest (QoI) of an engineering system, where $\mathcal{M}_c(\cdot|\boldsymbol{x}_c)$ is a deterministic simulator (e.g., a finite element code) with (deterministic) parameters $\boldsymbol{x}_c$. It follows that Y is a random variable which can be written as $Y = \mathcal{M}_s(\boldsymbol{Z}|\boldsymbol{X}_a, \boldsymbol{x}_c)$, where $\mathcal{M}_s := \mathcal{M}_c \circ \mathcal{M}_a$. Given this setting, it is easy to see that the conditional Cumulative Distribution Function (CDF) of Y given a realization $\boldsymbol{x_a}$ is simply

$$F_{Y|\boldsymbol{X}_a}(y|\boldsymbol{x_a}) = \mathbb{P}(\mathcal{M}_s(\boldsymbol{Z}|\boldsymbol{X}_a = \boldsymbol{x}_a) \leq y) = \int_{\boldsymbol{z}} \mathbb{I}\left(\mathcal{M}_s(\boldsymbol{z}|\boldsymbol{x}_a) \leq y\right) dF_{\boldsymbol{Z}}(\boldsymbol{z}), \tag{2}$$

where $\mathbb{I}(\cdot)$ denotes the indicator function, $\mathbb{P}(\cdot)$ denotes probability, $F_{\boldsymbol{Z}}(\boldsymbol{z})$ denotes the joint CDF.
Provided with $F_{Y|\boldsymbol{X}_a}$ continuous and strictly monotonically increasing, the p-quantile function is simply $y_p = F^{-1}_{Y|\boldsymbol{X}_a}(p|\boldsymbol{x_a})$. Observe that y_p is a random quantity as it is function of $\boldsymbol{X}_a$. Therefore, we can formally introduce the random variable Y_p as

$$Y_p = F^{-1}_{Y|\boldsymbol{X}_a}(p|\boldsymbol{X_a}) = \mathcal{M}_p(\boldsymbol{X}_a), \tag{3}$$

where $\mathcal{M}_p(\cdot) := F^{-1}_{Y|\boldsymbol{X}_a}(p|\cdot)$ is a deterministic model indexed by $p \in [0, 1]$. In this framework, Y_p (for different values of p) is the QoI used used for decision making.

In the proposed application, the computation of the statistics of Y_p is a complex and expensive computational problem. In fact, $\mathcal{M}_c$ is a computationally expensive black-box finite-element solver and, therefore, the evaluation of $\mathcal{M}_p$ is costly too.
Provided with such a setting, a surrogate model replaces the original model

$$\hat{Y}_p = \hat{\mathcal{M}}_p(\boldsymbol{X}), \tag{4}$$

where $\hat{Y}_p \approx Y_p$. The statistics of $\hat{Y}_p$ are, then, directly used for decision making. To define an optimal surrogate model w.r.t. the stochastic input, the computational solver, and QoI [29] designed a strategy that builds on PCE-based GSA and HK. Here, we summarize the main steps.

1. **Model definition and validation.** Define the QoI, the stochastic model of the input $\mathcal{M}_a$ (Section 4), and a set of structural simulators $\mathcal{M}_c$ (Section 3). In this application, $c \in \{LF, HF\}$, where LF stands for LF (state-space) structural simulator, and HF for HF (finite-element) structural simulator. The definition of the models follows the criteria reported in [29] and here synthesized.

   (a) The parameters of the stochastic model of the input are calibrated w.r.t. a hazard compatible site-specific seismic catalog.

   (b) The HF model has passed a *validation* protocol. This study uses HF models validated against HS tests performed in the laboratory of the University of Trento, Italy.

   (c) The LF model is a proxy of the HF model, which is computationally cheaper. In order to ensure the consistency required in a MF analysis ([29]), this study uses a LF model constructed via dynamic substructuring of the HF model [32].

2. **Initial experimental design.** Create a large Experimental Design (ED) $\{\boldsymbol{\mathcal{Y}}_{LF,p}, \boldsymbol{\mathcal{X}}_a\}$, where $\boldsymbol{\mathcal{Y}}_{LF,p} = \{y^{(1)}_{LF,p}, \ldots, y^{(N_{LF})}_{LF,p}\}$, $\boldsymbol{\mathcal{X}}_a = \{\boldsymbol{x}^{(1)}_a, \ldots, \boldsymbol{x}^{(N_{LF})}_a\}$, and $\boldsymbol{x}^{(n)}_a$ is a generic sample of the input parameters, and $y^{(n)}_{LF,p}$ is the corresponding LF estimate.

3. **PC-based global sensitivity analysis.** Train a non-intrusive PCE surrogate model, $\hat{\mathcal{M}}^{PCE}_{LF,p}(\boldsymbol{x}_a)$, using $\{\boldsymbol{\mathcal{Y}}_{LF,p}, \boldsymbol{\mathcal{X}_a}\}$, and perform a PCE-based GSA [35]. Retain the input random variables that contribute most to the variability (variance) of the QoI and fix the remaining ones to their expected value.

4. **Refined experimental design.** Train a reduced ED $\{\boldsymbol{\mathcal{Y}}_{HF,p}, \boldsymbol{\mathcal{X}}_{\alpha}\}$, where $\boldsymbol{\mathcal{Y}}_{HF,p} = \{y^{(1)}_{HF,p}, \dots, y^{(N_{HF})}_{HF,p}\}$, $\boldsymbol{\mathcal{X}}_{\alpha} = \{\boldsymbol{x}^{(1)}_{\alpha}, \dots, \boldsymbol{x}^{(N_{HF})}_{\alpha}\}$, and $\boldsymbol{x}^{(n)}_{\alpha}$ is a generic samples of the "important" model parameters, and $\boldsymbol{\mathcal{X}}_{\alpha}$ the collection of such samples.

5. **Kriging MF surrogate modelling.** Train a MF Kriging surrogate $\hat{\mathcal{M}}^{K}_{MF}(\boldsymbol{x}_{\alpha})$ based on $\{\boldsymbol{\mathcal{Y}}_{HF,p}, \boldsymbol{\mathcal{X}}_{\alpha}\}$, which uses the PCE surrogate as trend function.

6. **Probabilistic characterization of the QoI.** Compute the statistics of the QoI of interest via forward Monte-Carlo-based UQ analysis of the MF surrogate model.

In a PBEE setting, the QoI, Y_p, is usually an EDP. It follows that this framework allows the computation of any statistic of interest for the selected EDP, including fragility functions and surfaces w.r.t. any input variable included in $\boldsymbol{X}_a$.

3 A coupled tank-piping system case study

The tank-piping system represents a portion of an ideal CPP located in Hanford, California. As depicted in Figure 1, the piping system is connected to a slender steel tank through a bolted flange joint. In detail, the piping system comprises 8" (outer diameter: 219.08 mm; thickness: 8.18 mm) and 6" (outer diameter: 168.28 mm; thickness: 7.11 mm) tubes, two 90 deg elbows, one bolted flange joint and one tee joint. The steel tank is characterized by radius $R = 4.00$ m, height $H = 14.00$ m and thickness $T = 0.006$ m, and it is filled with a fluid of 900.00 kg/m^3 density. The system is subjected to a ground motion acceleration parallel to the main axis of the piping.

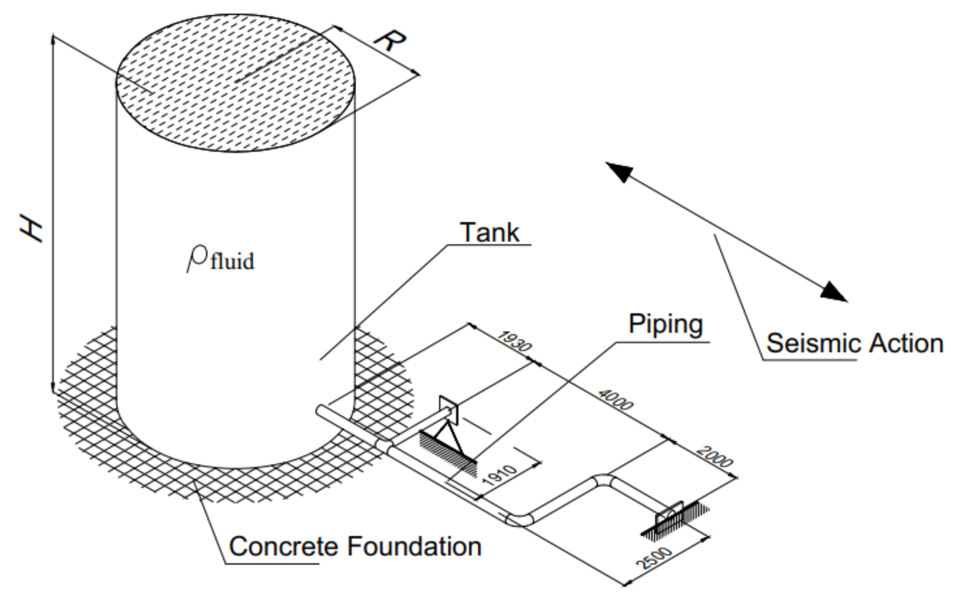

Figure 1: Tank-piping system case study.

In line with the presented framework, two structural simulators of the tank-piping system, characterized by different degrees of fidelity, were implemented. Both models assumed a linear elastic behavior for the piping system, which was discretized using 2D Euler-Bernoulli beam elements. Straight linear elastic 2D Euler-Bernoulli beams were also used for the elbow in the LF structural simulator, which was implemented in MATLAB. Joints and layouts significantly influence the overall piping vulnerability, as shown in different studies [36, 21, 20]. In particular, the occurrence of leakage is highly correlated to stress concentrations in pipe elbows, as highlighted in [19]. Hence, 3D shell-based elbow elements endowed with an elastoplastic constitutive law with kinematic hardening were used for the HF structural simulator. For a review of computational modeling issues related to piping bends, the reader is addressed to [37].
Both LF and HF structural simulators rely on the same simplified 3-DoFs tank model whose formulation is reported in [38]. An elastoplastic spring was used to model the Coulomb friction activated by tank sliding. The related cut-off force was computed based on the weight of the tank filled and a friction coefficient $\mu = 0.1$,

activated by a yield displacement of 1 mm. Table 1 summarizes the tank parameter values (i.e., $\boldsymbol{x}_c$). A *COMBIN40* element was used to implement the elastoplastic spring in the HF structural simulator in ANSYS, whereas the bilinear elastoplastic spring described in [39] was used for the LF structural simulator implemented in MATLAB.

Figure 2a reports a schematic of the LF structural simulator of the tank-piping system, whereas Figure 2b describes the collocation of 3D shell-based elbow elements in the HF structural simulator. Figure 2c reports the stress-strain relationship of the material constitutive law adopted for the steel of HF elbows.

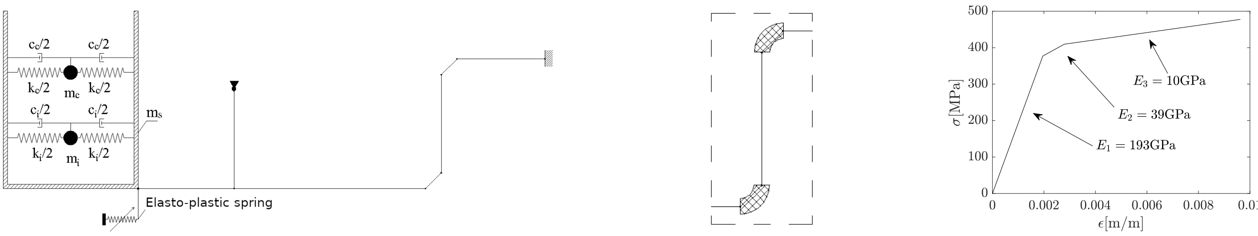

(a) (b) (c)

Figure 2: Computational modeling of the tank-piping system: a) schematic of the LF structural simulator; b) 3D shell-based elbow elements of the HF structural simulator; c) stress-strain relationship of steel constitutive law adopted in HF elbows.

Table 1: Simplified tank model parameters.

Parameter $\boldsymbol{x}_c$	Description	Value	Units
m_s	Sliding mass	22.91	ton
m_c	Convective mass	79.80	ton
m_i	Impulsive mass	547.00	ton
k_c	Convective stiffness	359	N/mm
k_i	Impulsive stiffness	685810	N/mm
ω_c	Convective frequency	2.12	rad/s
ω_i	Impulsive frequency	35.40	rad/s
ζ_c	Convective damping	0.005	–
ζ_i	Impulsive damping	0.05	–

The computational time needed for solving a single time history response analysis of the LF structural simulator was about 10 s. In contrast, a single evaluation of the time history response of the HF structural simulator was about 500 s. In detail, both cases refer to a 15 s long accelerogram using a standard laptop with an Intel 1.80 GHz i7-8565U CPU and 16 GB RAM.

4 Stochastic modeling of the seismic input

In this study, the AGM model proposed by Rezaian and Der Kiureghian [30, 40] was selected to represent the seismic input for the fragility analysis. This AGM model consists of a time-modulated band-limited non-stationary white noise described by the following equation,

$$A\left(t\right) = \mathcal{M}_a(t, \boldsymbol{Z}|\boldsymbol{X}_a) = q\left(t|\, \boldsymbol{X}_q\right) \frac{h(t|\boldsymbol{X}_h) * W\left(t, \boldsymbol{Z}\right)}{\sigma_h\left(t, \boldsymbol{Z}|\, \boldsymbol{X}_h\right)}, \tag{5}$$

where $*$ denotes time convolution; $\boldsymbol{X}_a = [\boldsymbol{X}_q, \boldsymbol{X}_h]$; $q\left(t|\, \boldsymbol{X}_q\right)$ is a parametric time modulating function with random parameters $\boldsymbol{X}_q$; $h(t|\boldsymbol{X}_h)$ is the impulse-response function of a linear filter with time varying random parameters, where $\boldsymbol{X}_h$ represents a set of time invariant parameters; $W(t, \boldsymbol{Z}) = \sum_n^{N_t} \delta(t - t_n) Z_n$ is a band-limited white noise process, where $\boldsymbol{Z} = [Z_1, ...Z_{N_t}]$ is a standard normal Gaussian vector; and $\sigma_h\left(t, \boldsymbol{Z}|\, \boldsymbol{X}_h\right)$ is the variance of the convoluted process up to time t. The modulating function proposed is,

$$q\left(t|\, \boldsymbol{X}_q\right) = \alpha_1 t^{\alpha_2 - 1} exp(-\alpha_3 t), \text{ if } t > 0, \text{ 0 elsewhere} \tag{6}$$

where $\boldsymbol{X}_q = [\alpha_1, \alpha_2, \alpha_3]$ are the parameters of the function. Moreover, it can be shown that a one-to-one mapping exists between these parameters and $D_{5-95} = T_{95} - T_5$, T_{45}, and I_a—where T_p is the time corresponding to the p % of the cumulative Arias intensity of the residual, $I_{a,res}$. It follows that $\boldsymbol{X}_q$ can be written as $\boldsymbol{X}_q = [I_{a,res}, T_{45}, D_{5-95}]$. The time-varying filter is defined by

$$h(t|\boldsymbol{X}_h) = \frac{\omega_f\,(t)}{\sqrt{1-\zeta_f^2}} \exp\left[-\omega_f\,(t)\,\zeta_f \cdot t\right] \sin\left[\omega_f\,(t)\sqrt{1-\zeta_f^2} \cdot t\right]. \tag{7}$$

In Eq.(7), the main frequency, $\omega_f(t)$, evolves linearly with time. Specifically, $\omega_f\,(t) = \omega_{mid} + \dot{\omega}\,(t - T_{45})$, where ω_{mid} is the frequency at time T_{45} and $\dot{\omega}$ is the rate of change of the frequency with time. The damping of the filter, ζ_f, is considered time invariant. It follows that $\boldsymbol{X}_h = [\omega_{mid}, \dot{\omega}, \zeta]$.

Unlike the original work [30, 40], AGM model parameters were calibrated for each real record of a selected pool instead of using regression analysis with respect to seismic hazard characteristics. In detail, based on the disaggregation of the seismic hazard corresponding to PGA with probability of exceedance of 2 % in 50 years, the seven ground motion records of the Northridge earthquake (California, 1994) reported in Table 2 were selected from the NGA database [41]. For both principal components of the selected ground motions, which were extracted according to the procedure described in [42], the AGM parameters were calibrated following the procedure reported in [40]. In this regard, Table 3 summarizes the obtained ranges of AGM model parameters.

Two sets of 4 and 3 artificial ground motions were selected to investigate system response within and beyond the linear regime. Specifically, based on nonlinear response analysis of the LF structural simulator, the first 4 accelerograms were selected to limit tank sliding peak to 0.04 m so that the piping response remained in the linear regime. These accelerograms are indicated as ELA #1-#4. Similarly, the other 3 accelerograms were selected to ensure a minimum tank sliding peak of 0.06 m, thus causing inelastic deformation of the elbows of the piping. These accelerograms are indicated as INE #1-#3. Figure 3 depicts acceleration, velocity, and displacement response spectra of both the real records and the artificial ground motions used for HS. The results of the HS campaign are discussed in Section 5.

Table 2: Selected records of the 1994 Northridge earthquake.

Station Name	Moment magnitude [M_w]	Epicentral distance [km]
Canoga Park - Topanga Can	6.69	14.70
Canyon Country - W Lost Cany	6.69	12.44
N Hollywood - Coldwater Can	6.69	12.51
Northridge - 17645 Saticoy St	6.69	12.09
Simi Valley - Katherine Rd	6.69	13.42
Sun Valley - Roscoe Blvd	6.69	10.05
Sunland - Mt Gleason Ave	6.69	13.35
Pacoima Kagel Canyon	6.05	11.34

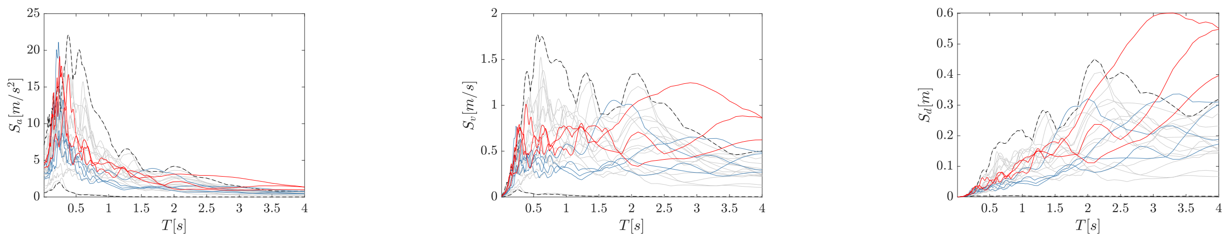

(a) (b) (c)

Figure 3: Selected records of the 1994 Northridge earthquake: a) acceleration; b) velocity; c) displacement response spectra. Grey lines refer to single retained records, whereas black dashed lines indicate the corresponding 95 % confidence interval. Blue and red lines indicate ELA and INE records produced with the calibrated AGM and used for the HS campaign.

Table 3: Intervals of the AGM model parameters.

Name	Lower bound	Upper bound	Units
I_a	1.019	3.992	m^2/s^3
D_{5-95}	5.083	16.810	s
T_{45}	1.596	5.664	s
ω_{mid}	14.620	31.000	rad/s
ζ	0.074	0.557	–

5 Model validation based on hybrid simulations

To support the validation of the HF finite-element model of the piping system, a HS campaign was performed at the University of Trento, Italy. In detail, the simplified model of the sliding tank (Section 3) constitutes the numerical substructure, and the piping system filled with 32 bar pressured water is the physical substructure. Figure 4 provides an overview of the experimental setup. Specifically, a hydraulic actuator of 250 kN force capacity and ±250 mm stroke was used to test the piping in displacement-control mode. A comprehensive description of the HS algorithm used in this experimental campaign is reported in [43]. As thoroughly discussed in [19], hoop strain is an effective indicator of the damage level experienced by pipe elbows. Accordingly, a set of strain gauges measured the hoop strain of each elbow, as depicted in Figure 5.

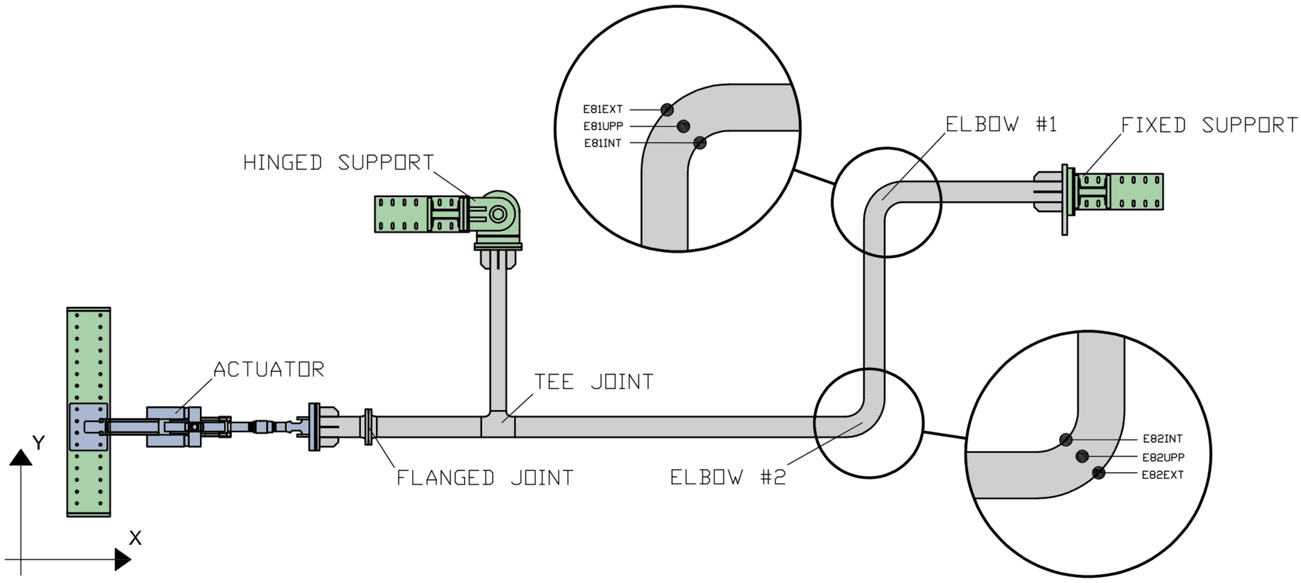

Figure 4: Schematic of the experimental setup. Labels *E81INT*, *E81EXT* and *E81UPP* indicate the strain gauges measuring the hoop strain of Elbow #1 at three different locations. Simularly, *E82INT*, *E82EXT* and *E82UPP* refer to Elbow #2.

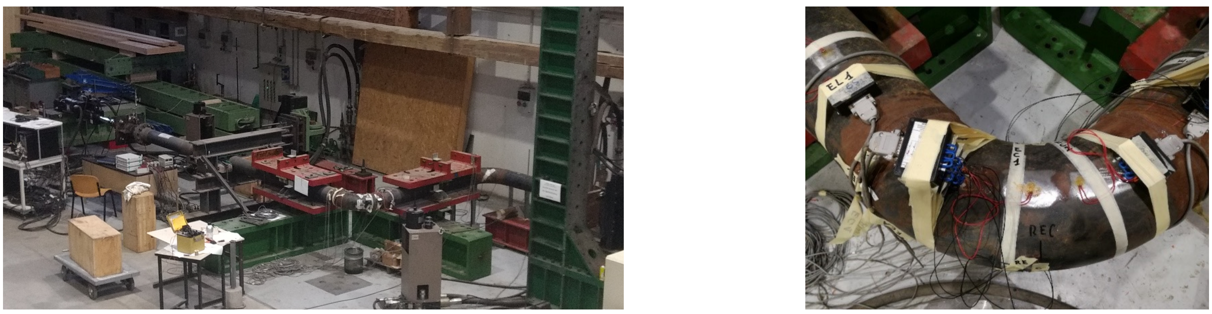

(a) (b)

Figure 5: Experimental setup: a) overview of the installation at the Laboratory of Structures and Materials of the University of Trento, Italy; b) close-up view of Elbow #2 instrumented with strain gauges.

The piping system was tested using HS considering the seven artificial accelerograms described in Section 4. Accordingly, artificial record labels ELA #1-#4 and INE #1-#3 are used to refer HS tests. In all cases, experiments were conducted in the so-called pseudodynamic regime considering a testing time scale equal to 64. Figures 6 and 7 provide an overview of the time history response of the piping system obtained via HS.

Figure 6 shows that the piping system response remained in the linear regime during HS tests ELA #1-#4. The slight hysteresis characterizing the restoring force can be ascribed to the friction between the piping and the Teflon support pads. Instead, Figure 7 shows that the response of the piping exceeded the linear regime during HS tests INE #1-#3. This observation is also confirmed by the measured strain histories.

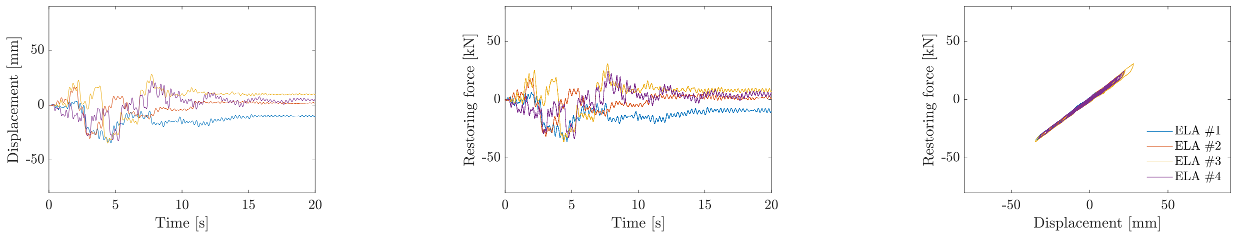

(a) (b) (c)

Figure 6: Experimental response of the piping obtained via HS during tests ELA #1-#4: a) displacement history; b) restoring force history; c) displacement vs. restoring force loop measured at the actuation point.

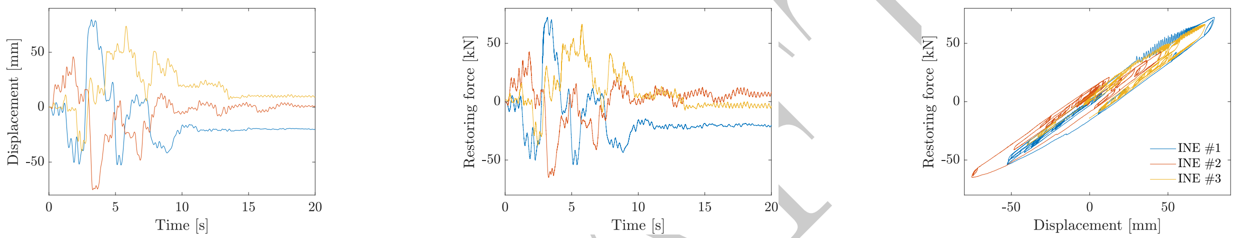

(a) (b) (c)

Figure 7: Experimental response of the piping obtained via HS during tests INE #1-#3: a) displacement history; b) restoring force history; c) displacement vs. restoring force loop measured at the actuation point.

The experimental response of the piping was used to calibrate the HF structural simulator, and in particular, the constitutive model for the steel material of elbow elements. In this regard, Figure 8 compares the hoop strain histories of Elbow #1 measured during HS to both LF and HF structural simulator predictions. Figure 8 shows that the *validated* HF structural simulator of the piping system accurately reproduces experimental measurements. On the other hand, a bias is observed in the LF prediction. The latter, however, effectively reproduces the time modulation of the hoop strain. It is, therefore, reasonable to leverage on few computationally expensive HF simulations to correct the bias of the response computed with the LF structural simulator.

6 Fragility analysis of the coupled tank-piping system

Provided with the notation introduced in this study, input variables and QoIs for the fragility analysis read

$$\boldsymbol{Y} = \epsilon_1 \ , \ \boldsymbol{X} \equiv \boldsymbol{X}_a = \{I_a, D_{5-95}, T_{45}, \omega_{mid}, \zeta\}, \tag{8}$$

where ϵ_1 indicates the hoop strain peak in Elbow #1. A constant value was assumed for $\dot{\omega}_{mid} = -0.568$ rad/s^2.

According to step 2 of the proposed framework, an initial ED of 200 samples was evaluated using the LF structural simulator and considering QoI quantiles $p = \{0.05 : 0.05 : 0.95\}$. To ensure stable quantile estimates up to 95 %, 100 realizations of the AGM were evaluated for each point of the ED for a total of 20,000 LF simulations. Then, PCE-based Sobol' sensitivity indices were computed. Tables 4 and 5 report PCE-based first-order and total Sobol' sensitivity indices related to Elbow #1. The contribution of I_a, ω_{mid} and ζ to the variability of Elbow #1 QoI is dominant for all quantiles. Therefore, they were retained as input variables for the subsequent HK surrogate modeling phase. The remaining parameters of the AGM were set to constant average values $D_{5-95} = 10.44$ s and $T_{45} = 3.70$ s. For the sake of brevity, only quantiles $p = \{0.1 : 0.1 : 0.9\}$ are

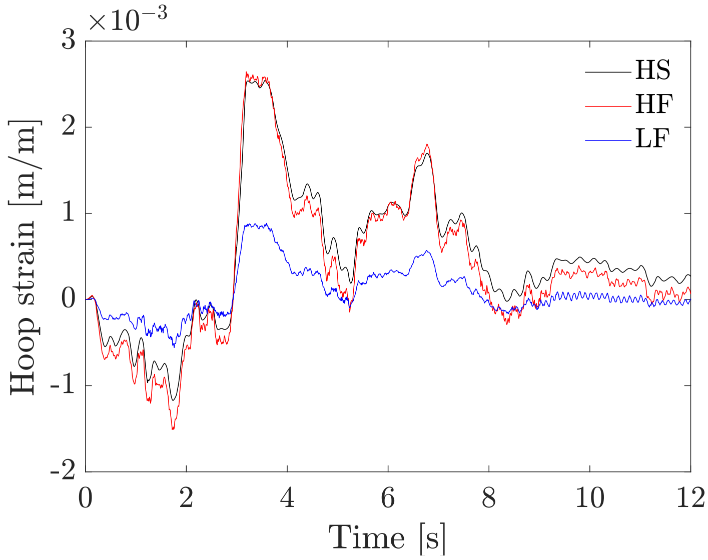

Figure 8: Hoop strain history of Elbow #1 measured by sensor *E81UPP* during the HS test INE #2 and corresponding LF and HF simulations.

reported. Tables 4 and 5 report also leave-one-out errors ε_{loo} to report the accuracy of PCE surrogates. In the case of regression-based PCE, ε_{loo} can be directly calculated from the coefficients of the PCE computed with the *entire* ED [44].

Table 4: First-order PCE-based Sobol' indices of the hoop strain peak of Elbow #1 (QoI).

p	ε_{loo}	I_a	D_{5-95}	T_{45}	ω_{mid}	ζ
0.000	0.036	0.750	0.016	0.000	0.102	0.050
0.100	0.006	0.690	0.023	0.004	0.112	0.083
0.200	0.004	0.678	0.028	0.004	0.107	0.093
0.300	0.004	0.668	0.029	0.005	0.114	0.094
0.400	0.004	0.656	0.030	0.006	0.114	0.101
0.500	0.005	0.641	0.032	0.008	0.117	0.108
0.600	0.004	0.630	0.034	0.009	0.118	0.112
0.700	0.004	0.616	0.039	0.011	0.119	0.117
0.800	0.005	0.612	0.036	0.013	0.117	0.123
0.900	0.007	0.596	0.036	0.016	0.119	0.131

Table 5: Total PCE-based Sobol' indices of the hoop strain peak of Elbow #1 (QoI).

p	ε_{loo}	I_a	D_{5-95}	T_{45}	ω_{mid}	ζ
0.000	0.036	0.823	0.030	0.010	0.145	0.084
0.100	0.006	0.772	0.034	0.005	0.157	0.122
0.200	0.004	0.763	0.041	0.006	0.148	0.138
0.300	0.004	0.751	0.044	0.007	0.152	0.137
0.400	0.004	0.740	0.045	0.009	0.152	0.148
0.500	0.005	0.727	0.047	0.011	0.156	0.157
0.600	0.004	0.718	0.050	0.012	0.157	0.163
0.700	0.004	0.703	0.056	0.014	0.158	0.169
0.800	0.005	0.698	0.055	0.019	0.156	0.173
0.900	0.007	0.683	0.055	0.026	0.156	0.184

Among retained parameters, first-order summands of Figure 9 highlight monotonic increasing relationships with the QoI only for I_a and ζ. Hence, they were employed as IMs for computing the fragility analysis.

According to step 3 of the computational framework, a refined ED of 20 samples was evaluated using the

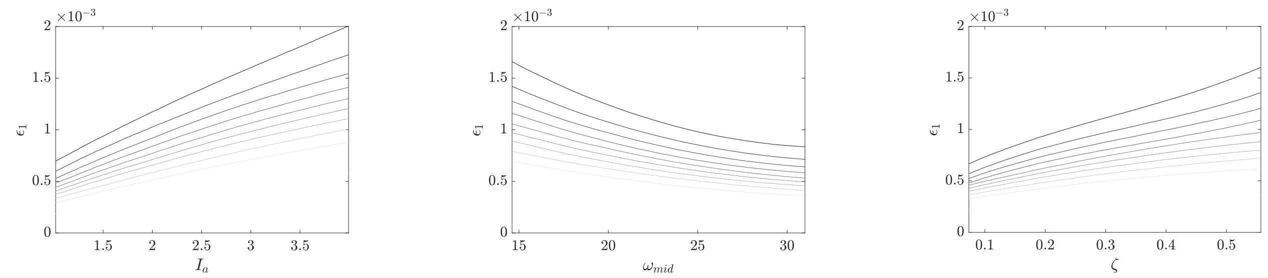

(a) (b) (c)

Figure 9: First-order summands of the hoop strain peak ϵ_1 of Elbow #1 (QoI) for the quantiles reported in Tables 4 and 5. Lighter curves refer to quantile $p = 0.1$ while darker curves refer to quantile $p = 0.9$.

HF structural simulator considering,

$$\boldsymbol{X}_\alpha = \{I_a, \omega_{mid}, \zeta\} \ , \boldsymbol{x}_\beta = E\left[\{T_{45}, D_{5-95}\}\right]. \tag{9}$$

For each sample of the refined ED, 100 AGM realizations were evaluated for a total of 2,000 HF simulations. Then, HK surrogates were trained for different ED sizes. Accordingly, HK-n indicates a HK surrogate computed with n samples of the HF structural simulator response quantiles. The PCE surrogate trained on the LF simulator was used as a trend function for the HK surrogates. A Matérn 5/2 correlation function $R\left(\boldsymbol{X} - \boldsymbol{X}'|\boldsymbol{\theta}\right)$ and second-order polynomial trend function $\boldsymbol{\mu}\left(\boldsymbol{X}\right)$ were adopted.

The fragility models reported in Figures 10a and 10b were computed via Monte-Carlo-based UQ analysis using surrogate models assuming an hoop strain threshold value $\epsilon_y = 1.70 \times 10^{-3}$, which is associated with the yielding serviceability limit state [45]. More precisely, the fragility curves of Figure 10a adopt I_a as IM and were obtained based on the PCE surrogate of the LF structural simulator and three HK surrogates. As can be observed, curves are already stable with 18 HF samples. The fragility surface of Figure 10b adopts I_a and ζ as IMs and was obtained from the HF-20 kriging surrogate. Specifically, the fragility curves reported in Figure 10a were obtained from the PCE surrogate of the LF simulator and three HK surrogates of the HF simulator. In the latter case, the three HK surrogates were obtained considering 18, 19, and 20 samples of the HF simulator response; hence, they are indicated as HK-18, HK-19, and HK-20, respectively. As can be observed, fragility curves approach a stable shape already with 18 samples of the HF simulator response. The motivation behind the selection of I_a as IM for the fragility curves is twofold. First, I_a is associated with the larger Sobol' sensitivity index and, therefore, it is the most sensitive parameter of the LF simulator; see, Tables 4 and 5 in this respect. Moreover, according to Figure 9a, I_a shows a monotonic increasing relationship with the selected EDP. On the other hand, the fragility surface of Figure 10b was obtained for the HK surrogate indicated as HK-20. Owing to their substantial contribution to the variability of the EDP demonstrated by Sobol' indices, I_a and ζ were selected as IMs. Moreover, according to Figures 9a and 9c, both these two parameters show a monotonic increasing relationship with the EDP.

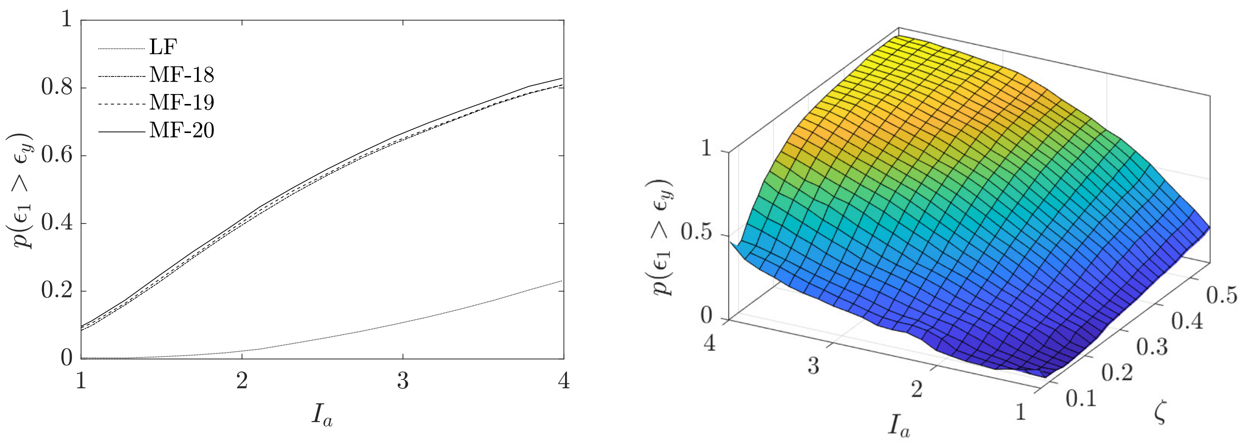

(a) (b)

Figure 10: Fragility models for the yielding limit state of Elbow #1 assuming a hoop strain threshold value $\epsilon_y = 1.70 \times 10^{-3}$: a) fragility curve; b) fragility surface.

Although both LF and HF EDs assumed independent uniformly distributed AGM input parameters, fragility models can be easily resampled considering a joint PDF calibrated for the specific seismic hazard. Also, AGM input parameters can be mapped to instrumental IM, as illustrated in [46].

7 Conclusions

This study presented the application of a novel computational framework for fragility analysis of a prototype tank-piping system. The framework is selected because it addresses the following criticalities associated with the current fragility analysis practice: i- scarcity of hazard-specific site-consistent ground motion records, ii- high computational cost of high-fidelity simulations, iii- high experimental cost of model validation. In detail, the framework uses i- a stochastic ground motion model to augment the number of time series, ii- extensive use of surrogate and multi-fidelity modeling to drastically reduce the computational cost, iii- hybrid simulation tests to validate the computational models at a reduced experimental cost.

A realistic coupled tank-piping system was used to illustrate the application of the framework to chemical process plants. Fragility models related to yielding limit state were computed for one elbow of the piping system using multi-fidelity surrogate modeling. This method builds on a combination of low-and high- fidelity computational models. The latter was validated against hybrid simulation experiments. The same stochastic ground motion model was used for producing artificial records both for hybrid simulation and fragility analysis. The results highlight the great flexibility and potential of the method for a fragility assessment of chemical process plant components.

Noteworthy, piping elbows were neither replaced nor repaired during the presented experimental campaign. This was possible because the piping response barely exceeded the linear regime. Future research will try to minimize the number of hybrid simulation tests necessary to produce accurate fragility models for plant components exposed to large plastic strains.

8 Acknowledgements

The authors wish to acknowledge Dr. Stefano Marelli (Chair of Risk, Safety and Uncertainty Quantification, ETH Zurich) and Dr. Imad Abdallah (Chair of Structural Mechanics, ETH Zurich) for providing constructive comments during the preparation of this manuscript. Also, the EU SERA project (Grant No. 730900) is acknowledged. Finally, the second, the third, and the last authors were supported by the Italian Ministry of Education, University and Research (MIUR) in the frame of the "Departments of Excellence" (grant L 232/2016).

References

[1] M. Campedel, "Analysis of Major Industrial Accidents Triggered by Natural Events Reported In the Principal Available Chemical Accident Databases," tech. rep., European Commission, Joint Research Centre, Institute for the Protection and the Security of the Citizen, 2008.

[2] K. Kidam and M. Hurme, "Analysis of equipment failures as contributors to chemical process accidents," *Process Safety and Environmental Protection*, vol. 91, no. 1-2, pp. 61–78, 2013.

[3] A. M. Cruz, L. J. Steinberg, and A. L. Vetere-Arellano, "Emerging Issues for Natech Disaster Risk Management in Europe," *Journal of Risk Research*, vol. 9, no. 5, pp. 483–501, 2006.

[4] L. J. Steinberg, H. Sengul, and A. M. Cruz, "Natech risk and management: an assessment of the state of the art," *Natural Hazards*, vol. 46, no. 2, pp. 143–152, 2008.

[5] H. Sezen and A. S. Whittaker, "Seismic Performance of Industrial Facilities Affected by the 1999 Turkey Earthquake," *Journal of Performance of Constructed Facilities*, vol. 20, no. 1, pp. 28–36, 2006.

[6] E. Krausmann, A. M. Cruz, and B. Affeltranger, "The impact of the 12 May 2008 Wenchuan earthquake on industrial facilities," *Journal of Loss Prevention in the Process Industries*, vol. 23, no. 2, pp. 242–248, 2010.

[7] P. Y. Lipscy, K. E. Kushida, and T. Incerti, "The Fukushima Disaster and Japan's Nuclear Plant Vulnerability in Comparative Perspective," *Environmental Science & Technology*, vol. 47, no. 12, pp. 6082–6088, 2013.

[8] E. Salzano, I. Iervolino, and G. Fabbrocino, "Seismic risk of atmospheric storage tanks in the framework of quantitative risk analysis," *Journal of Loss Prevention in the Process Industries*, vol. 16, no. 5, pp. 403–409, 2003.

[9] G. Fabbrocino, I. Iervolino, F. Orlando, and E. Salzano, "Quantitative risk analysis of oil storage facilities in seismic areas," *Journal of Hazardous Materials*, vol. 123, no. 1-3, pp. 61–69, 2005.

[10] G. Lanzano, E. Salzano, F. Santucci de Magistris, and G. Fabbrocino, "Seismic vulnerability of natural gas pipelines," *Reliability Engineering & System Safety*, vol. 117, pp. 73–80, 2013.

[11] G. Lanzano, F. Santucci de Magistris, G. Fabbrocino, and E. Salzano, "Seismic damage to pipelines in the framework of Na-Tech risk assessment," *Journal of Loss Prevention in the Process Industries*, vol. 33, pp. 159–172, 2015.

[12] Task Committee on Seismic Evaluation and Design of Petrochemical Facilities of ASCE, *Guidelines for Seismic Evaluation and Design of Petrochemical Facilities.* Reston, VA: American Society of Civil Engineers, second edition ed., 2011.

[13] S. Esposito, B. Stojadinović, A. Babič, M. Dolšek, S. Iqbal, J. Selva, M. Broccardo, A. Mignan, and D. Giardini, "Risk-Based Multilevel Methodology to Stress Test Critical Infrastructure Systems," *Journal of Infrastructure Systems*, vol. 26, no. 1, p. 04019035, 2020.

[14] A. C. Caputo, F. Paolacci, O. S. Bursi, and R. Giannini, "Problems and Perspectives in Seismic Quantitative Risk Analysis of Chemical Process Plants," *Journal of Pressure Vessel Technology*, vol. 141, no. 1, p. 010901, 2019.

[15] L. Di Sarno and G. Karagiannakis, "Petrochemical Steel Pipe Rack: Critical Assessment of Existing Design Code Provisions and a Case Study," *International Journal of Steel Structures*, vol. 20, no. 1, pp. 232–246, 2020.

[16] M. Hosseini, E. Ghalyani, and N. G. Amirabad, "Development of double-variable seismic fragility functions for oil refinery piping systems," *Journal of Loss Prevention in the Process Industries*, p. 104259, 2020.

[17] A. Mebarki, "Safety of atmospheric industrial tanks: fragility, resilience and recovery functions," *Journal of Loss Prevention in the Process Industries*, vol. 49, pp. 590–602, 2017.

[18] H. N. Phan, F. Paolacci, O. S. Bursi, and N. Tondini, "Seismic fragility analysis of elevated steel storage tanks supported by reinforced concrete columns," *Journal of Loss Prevention in the Process Industries*, vol. 47, pp. 57–65, 2017.

[19] O. S. Bursi, R. di Filippo, V. La Salandra, M. Pedot, and M. S. Reza, "Probabilistic seismic analysis of an LNG subplant," *Journal of Loss Prevention in the Process Industries*, vol. 53, pp. 45–60, 2018.

[20] L. Di Sarno and G. Karagiannakis, "On the seismic fragility of pipe rack—piping systems considering soil–structure interaction," *Bulletin of Earthquake Engineering*, vol. 18, no. 6, pp. 2723–2757, 2020.

[21] O. S. Bursi, M. S. Reza, G. Abbiati, and F. Paolacci, "Performance-based earthquake evaluation of a full-scale petrochemical piping system," *Journal of Loss Prevention in the Process Industries*, vol. 33, pp. 10–22, 2015.

[22] O. S. Bursi, F. Paolacci, M. S. Reza, S. Alessandri, and N. Tondini, "Seismic assessment of petrochemical piping systems using a performance-based approach," *Journal of Pressure Vessel Technology*, vol. 138, no. 3, 2016.

[23] M. Farhan and S. Bousias, "Seismic fragility analysis of lng sub-plant accounting for component dynamic interaction," *Bulletin of Earthquake Engineering*, vol. 18, no. 10, pp. 5063–5085, 2020.

[24] D. Vamvatsikos and C. A. Cornell, "Incremental dynamic analysis," *Earthquake Engineering & Structural Dynamics*, vol. 31, no. 3, pp. 491–514, 2002.

[25] K. Porter, R. Kennedy, and R. Bachman, "Creating Fragility Functions for Performance-Based Earthquake Engineering," *Earthquake Spectra*, vol. 23, no. 2, pp. 471–489, 2007.

[26] J. W. Baker, "Efficient Analytical Fragility Function Fitting Using Dynamic Structural Analysis," *Earthquake Spectra*, vol. 31, no. 1, pp. 579–599, 2015.

[27] B. A. Bradley, "A critical examination of seismic response uncertainty analysis in earthquake engineering," *Earthquake Engineering & Structural Dynamics*, vol. 42, no. 11, pp. 1717–1729, 2013.

[28] V. Silva, S. Akkar, J. Baker, P. Bazzurro, J. M. Castro, H. Crowley, M. Dolsek, C. Galasso, S. Lagomarsino, R. Monteiro, D. Perrone, K. Pitilakis, and D. Vamvatsikos, "Current Challenges and Future Trends in Analytical Fragility and Vulnerability Modeling," *Earthquake Spectra*, vol. 35, no. 4, pp. 1927–1952, 2019.

[29] G. Abbiati, M. Broccardo, I. Abdallah, S. Marelli, and F. Paolacci, "Seismic fragility analysis based on artificial ground motions and surrogate modeling of validated structural simulators," 2020.

[30] S. Rezaeian and A. Der Kiureghian, "A stochastic ground motion model with separable temporal and spectral nonstationarities," *Earthquake Engineering & Structural Dynamics*, vol. 37, no. 13, pp. 1565–1584, 2008.

[31] A. H. Schellenberg, S. A. Mahin, and G. L. Fenves, "Advanced Implementation of Hybrid Simulation," Tech. Rep. PERR 2009/104, Pacific Earthquake Engineering Research (PEER) Center, University of California, Berkeley, 2009.

[32] D. de Klerk, D. J. Rixen, and S. N. Voormeeren, "General Framework for Dynamic Substructuring: History, Review and Classification of Techniques," *AIAA Journal*, vol. 46, no. 5, pp. 1169–1181, 2008.

[33] I. Gidaris, A. A. Taflanidis, and G. P. Mavroeidis, "Kriging metamodeling in seismic risk assessment based on stochastic ground motion models," *Earthquake Engineering & Structural Dynamics*, vol. 44, no. 14, pp. 2377–2399, 2015.

[34] S. Ghosh, A. Roy, and S. Chakraborty, "Kriging Metamodeling-Based Monte Carlo Simulation for Improved Seismic Fragility Analysis of Structures," *Journal of Earthquake Engineering*, pp. 1–21, 2019.

[35] B. Sudret, "Global sensitivity analysis using polynomial chaos expansions," *Reliability Engineering & System Safety*, vol. 93, no. 7, pp. 964–979, 2008.

[36] G. DeGrassi, "Seismic Analysis of Large-Scale Piping Systems for the JNES-NUPEC Ultimate Strength Piping Test Program (NUREG/CR-6983)," tech. rep., Office of Nuclear Regulatory Research, US Nuclear Regulatory Commission, 2008.

[37] S. A. Karamanos, "Mechanical Behavior of Steel Pipe Bends: An Overview," *Journal of Pressure Vessel Technology*, vol. 138, no. 4, p. 041203, 2016.

[38] P. K. Malhotra, T. Wenk, and M. Wieland, "Simple Procedure for Seismic Analysis of Liquid-Storage Tanks," *Structural Engineering International*, vol. 10, no. 3, pp. 197–201, 2000.

[39] N. Mostaghel, "Analytical Description of Pinching, Degrading Hysteretic Systems," *Journal of Engineering Mechanics*, vol. 125, no. 2, pp. 216–224, 1999.

[40] S. Rezaeian and A. Der Kiureghian, "Simulation of synthetic ground motions for specified earthquake and site characteristics," *Earthquake Engineering & Structural Dynamics*, pp. n/a–n/a, 2010.

[41] B. Chiou, R. Darragh, N. Gregor, and W. Silva, "NGA Project Strong-Motion Database," *Earthquake Spectra*, vol. 24, no. 1, pp. 23–44, 2008.

[42] J. W. Baker, "Quantitative classification of near-fault ground motions using wavelet analysis," *Bulletin of the Seismological Society of America*, vol. 97, no. 5, pp. 1486–1501, 2007.

[43] G. Abbiati, I. Lanese, E. Cazzador, O. S. Bursi, and A. Pavese, "A computational framework for fast-time hybrid simulation based on partitioned time integration and state-space modeling," *Structural Control and Health Monitoring*, vol. 26, no. 10, p. e2419, 2019.

[44] M. Berveiller, B. Sudret, and M. Lemaire, “Stochastic finite element: a non intrusive approach by regression,” *European Journal of Computational Mechanics*, vol. 15, no. 1-3, pp. 81–92, 2006.

[45] B. Liu, X. Liu, and H. Zhang, “Strain-based design criteria of pipelines,” *Journal of Loss Prevention in the Process Industries*, vol. 22, pp. 884–888, 2009.

[46] A. Suzuki and I. Iervolino, “Intensity measure conversion of fragility curves,” *Earthquake Engineering & Structural Dynamics*, vol. 49, no. 6, pp. 607–629, 2020.